Time-energy properties of an attosecond extreme ultra-violet pulse*

Ge Yu-Cheng(葛愉成)† and He Hai-Ping(何海萍)

School of Physics and Key Laboratory of Nuclear Physics and Technology, Peking University, Beijing 100871, *China*

(Received 29 April 2010; revised manuscript received 13 July 2010)

The time-energy properties of high-order harmonic generation (HHG) are calculated for a linearly polarized 7-fs laser pulse with different carrier-envelope phases (CEPs). The quantum trajectory paths that contribute to an as (1 as=10^{-18} s) pulse in HHG are identified. The laser-duration dependence and the CEP dependence of HHG energy property are investigated. The study shows that an as extreme ultra-violet (XUV) pulse can be selected from HHG spectrum near cut-off energy with a bandpass optical filter. The theoretical prediction of the pulse duration is proportional to bandwidth. Analysis suggests that a measured narrowband as XUV pulse may consist of instantaneous shorter pulses each dependent on laser pulse duration, intensity, and CEP. These information can be used as references for producing, selecting, improving and manipulating (timing) as pulses.

Keywords: high harmonic generation, energy properties, attosecond pulse, carrier envelope phase

PACC: 3365, 3280F, 3280, 3365C

1. Introduction

High-order harmonic generation (HHG) has been a successful way to produce as (1 as=10^{-18} s) extreme ultra-violet (XUV) pulses[1−9] and the x-ray pulses in the water window (photon energies ranging from 283.7 eV to 532.1 eV, or wavelengths between 2.33 nm to 4.37 nm) which are useful in biochemical research.[10,11] Although the lack of required non-linear optical effects makes it difficult to directly measure the temporal properties of an as XUV pulse by conventional methods, they can be determined by analysing the photo-electron spectra measured using laser-assisted photo-ionizations. Recently, different techniques such as phase-matching and spatial filtering have been used for analysing, producing and selecting an isolated as pulse by HHG.[12−14] The latest measurement of an as pulse duration is 80 as.[15] However, people never stop improving the production of and seeking for new methods to reconstruct an isolated as pulse at higher photon energies and shorter duration for use.[16−27] Except for the laser intensity, the wavelength and the pulse shape that instantaneously determine the HHG spectrum, the laser carrier-envelope phase (CEP) is another important parameter that affects both HHG and laser-assisted photo-ionization.[28−30] In experiment, technical limitation inevitably yields pulse jitter, parameter fluctuations and walks over the course of a long experiment. Pulse selection, transportation and interaction with medium also result in modification and deformation of the pulse profile. This motivated us to quantitatively investigate the detailed temporal properties of the pulse. Since HHG refers to quantum processes of atoms in strong fields, our investigation is based on the calculations of the HHG energy properties at the single-atom level by using the strong field approximation (SFA).[31]

According to the Lewenstein's theory,[31] the HHG can be explained in terms of quantum trajectories, each with its own amplitude and the radiation energy. It is very interesting to look into these trajectories and identify those which contribute to an as pulse. Similar to an HHG intensity spectrum that describes distribution of the radiation amplitudes at different photon energies, the calculated HHG energy properties describe a photon energy distribution in time or laser phase domain, which can be measured as a sum of contributions from atoms in the field. The study shows that these HHG energy properties provide new references for producing and selecting an isolated as pulse with a specified bandwidth. However, such a calculation gives only a theoretical prediction of the pulse duration. Many factors affect the time profile of

*Project supported by the National Natural Science Foundation of China (Grant Nos. 10827505 and 10675014).

†Corresponding author. E-mail: gyc@pku.edu.cn

© 2010 Chinese Physical Society and IOP Publishing Ltd

the measured pulse, such as the beam size, the interactions of both the laser and the generated pulse with the media and their transportation, etc. Instabilities of laser pulse duration, intensity, and CEP also affect HHG and as measurements. Beam jitter, parameter fluctuation, and beam walk over the course of a long experiment may alter each as pulse. As the pulse becomes shorter and the bandwidth narrower, it is useful to see how these factors affect the result.

The rest of the present paper is organized as follows. In Section 2, the HHG radiation energy properties are calculated for a linearly-polarized laser pulse with a 7-fs (1 fs=10^{-15} s) duration. The time profile of an isolated single XUV pulse is quantitatively investigated. In Section 3, factors affecting the result of pulse detection are discussed. In Section 4, the obtained findings are given.

2. Time properties of an isolated narrowband XUV pulse

HHG refers to a non-perturbative quantum process of an atom in a strong laser field. We use the saddle-point method[1−9] to calculate the HHG energy properties and observe the factors they depend on.

2.1. Saddle-point method

The electron motion of an atom in a strong laser field ($\boldsymbol{E}(t)$) satisfies the time-dependent Shrödinger equation (TDSE),

$$\mathrm{i}\frac{\partial}{\partial t}\Psi(\boldsymbol{r},t) = \left[-\frac{1}{2}\nabla^2 - \frac{1}{r} - \boldsymbol{r}\cdot\boldsymbol{E}(t)\right]\Psi(\boldsymbol{r},t), \quad (1)$$

where $\Psi(\boldsymbol{r},t)$ is the electron wave function, $\boldsymbol{r} = (x,y,z)$ represents the electron space coordinates, and t denotes time. $\boldsymbol{E}(t) = E_0F(t)\cos(\omega_{\mathrm{L}}t+\Phi)$ (x direction) describes a linearly-polarized laser field for HHG, where E_0 is the amplitude of the field; $F(t)$ is the laser envelope, e.g. a Gaussian shape function; ω_{L} is the laser angular frequency, and Φ is the CEP. The system is initially in the ground state. Atomic units and hydrogen atoms are used for simplicity.

According to the Lewenstein's theory and the saddle point method,[31] the only relevant electron trajectories that contribute to HHG are those where the electron leaves the nucleus at birth time t' and returns to the same place at recombination time t (the return time $\tau = t - t'$). This is the HHG space condition, expressed by $\nabla_{\mathrm{p}}\widetilde{S}(\boldsymbol{p},t,\tau) = \boldsymbol{r}(t) - \boldsymbol{r}(t') = 0$. Here, $\widetilde{S}(\boldsymbol{p},t,\tau)$ is defined as the quasi-classical action

$$\widetilde{S}(\boldsymbol{p},t,\tau) = \int_{t'}^{t}\mathrm{d}t''\left\{\frac{[\boldsymbol{p}-\boldsymbol{A}(t'')]^2}{2} + I_{\mathrm{p}}\right\}, \quad (2)$$

where $\boldsymbol{p}$ is the electron canonical momentum, $\boldsymbol{A}(t'')$ is the vector potential of the laser field ($\boldsymbol{E}(t) = -(1/c)\partial_t\boldsymbol{A}(t)$, and c is the velocity of light in vacuum). $\widetilde{S}(\boldsymbol{p},t,\tau)$ describes the phase that an electron gains in the laser field. The dominant contribution to the harmonic radiation comes from a trajectory that satisfies the time condition $\partial\widetilde{S}(\boldsymbol{p},t,\tau)/\partial\tau = 0$. The space condition and the time condition are used to determine the saddle point at the canonical momentum $\boldsymbol{p}_{\mathrm{st}}$ and the return time τ_{st}, respectively. The harmonic energy can be calculated with $(2K+1)\hbar\omega_{\mathrm{L}} = \partial\widetilde{S}(\boldsymbol{p},t,\tau)/\partial t = [\boldsymbol{p}-\boldsymbol{A}(t)]^2/2 + I_{\mathrm{p}}$, where $2K+1$ is the order of harmonic radiation, I_{p} is the atomic potential, and $E_{\mathrm{kin}}(t) \equiv [\boldsymbol{p}-\boldsymbol{A}(t)]^2/2$ is the kinetic energy that an electron gains in the laser field.

In the following analysis, $E_{\mathrm{kin}}(t)$ is calculated with the saddle point method in the case of $I_{\mathrm{p}}/U_{\mathrm{p}} \approx 0$, where $U_{\mathrm{p}} = E_0^2/4\omega_{\mathrm{L}}^2$ is the ponderomotive potential of the laser field. U_{p} is proportional to the laser intensity $S = E_0^2/2$. $E_{\mathrm{kin}}(t)$ serves as the radiation energy property at time t. The generated harmonic photon energy is $\hbar\omega_X = E_{\mathrm{kin}}(t) + I_{\mathrm{p}}$, where ω_X is the XUV angular frequency. In calculations, we use $F(t) = \exp(-4\ln 2\cdot t^2/\tau_{\mathrm{L}}^2)$, where τ_{L} is the laser pulse duration in full width at half maximum (FWHM).

2.2. HHG energy properties

Figure 1(a) illustrates the laser carrier field function $F(t)\cos(\omega_{\mathrm{L}}t+\Phi)$ (x direction, amplitude 1, shown by thin solid line) and $F(t)$ (dash line) with $\tau_{\mathrm{L}} = 7$ fs, $\Phi = 0°$ and the wavelength $\lambda_{\mathrm{L}} = 750$ nm. The shade circle G denotes the time position where the highest order harmonic is generated. The heavy solid line and the dot line plot the shifted quasi-classical action, $\widetilde{S}(\boldsymbol{p},0.49,\tau = 0.49-t)/3 + 0.32$, and the kinetic energy, $E_{\mathrm{kin}}(t)$ (shown by $E_{\mathrm{kin}}(t)/U_{\mathrm{p}} + 0.32$), of an electron ionized at time t' (< 0.49 fs) and recombined with the ion at G ($t = 0.49$ fs), respectively. Harmonics are radiated by electrons ionized at stationary points denoted by open circles A', B', C', and D' on the heavy solid line where $\partial\widetilde{S}(\boldsymbol{p},0.49,\tau = 0.49-t)/\partial\tau = 0$, and recombined with the ion at G. The kinetic energies of these electrons are values peaked at open circles A'', B'', C'', and D'' denoted on the dot line. Open circles

A, B, C, and D on the thin solid line temporally correspond to A', B', C', and D', respectively. Particularly, the electron ionized at A ($t = -0.13$ fs) (stationary point A') and recombined at G radiates the highest energy harmonic, $(2K+1)_{\max}\hbar\omega_{\rm L} = 3.0U_{\rm p} + I_{\rm p}$. The electrons ionized at B, C, and D (other stationary points B', C' and D'), and recombined at G, radiate harmonics of less energies.

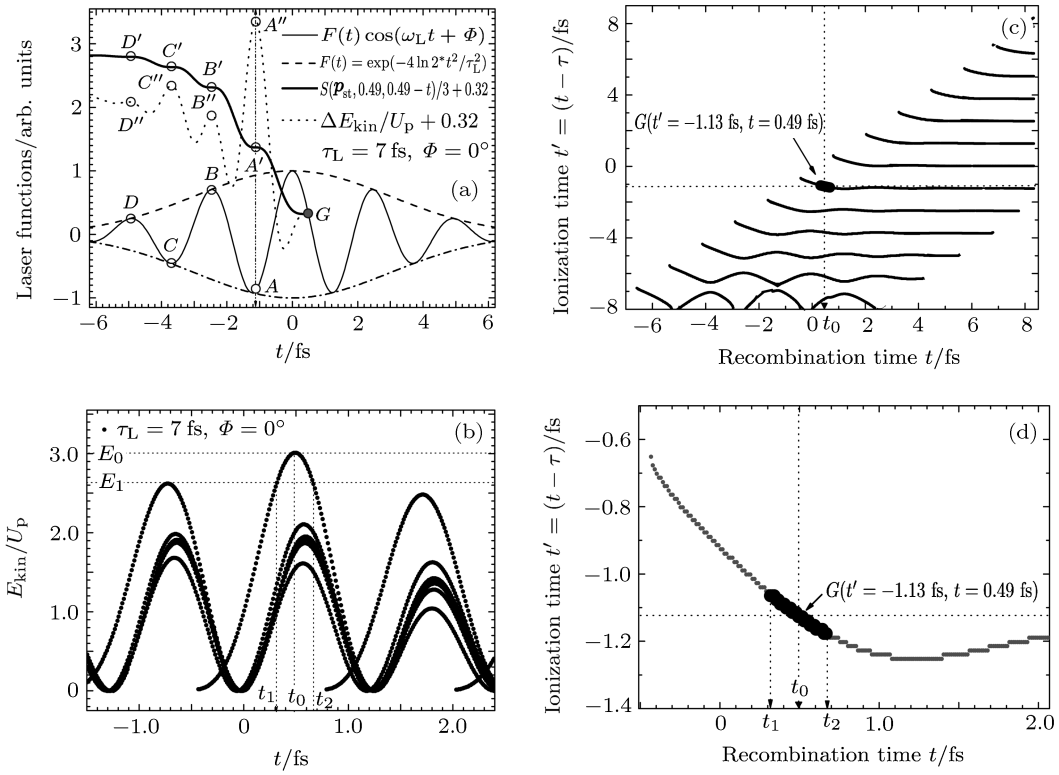


Fig. 1. (a) Illustration of HHG. Thin solid and dash lines represent the laser field function $F(t)\cos(\omega_{\rm L}t+\Phi)$ (x direction, amplitude 1) and its envelope $F(t)$, respectively. Heavy solid line: shifted quasi-classical action, $\widetilde{S}(\boldsymbol{p}_{\rm st}, 0.49, 0.49-\tau)/3+0.32$. Dot line: shifted electron kinetic energy, $E_{\rm kin}(t)$ (shown by $E_{\rm kin}(t)/U_{\rm p}+0.32$). Shade circle G: the temporal position where the highest order harmonic is generated. Open circles $A\sim D$, $A'\sim D'$ and $A''\sim D''$: the saddle points refer to the laser field, quasi-classical action, and electron kinetic energy, respectively, when electrons are ionized and then recombined with ions at G. (b) Energy properties of HHG. Solid circles: the electron kinetic energy $E_{\rm kin}(t)$ as a function of t, calculated for a linearly-polarized laser with $\tau_{\rm L} = 7$ fs and $\Phi = 0°$. (c) Stationary points of different values of t' and t. Point G is identical to that in (a). (d) An expanded area of (c).

Figure 1(b) depicts the HHG energy properties calculated with the same laser as that in Fig. 1(a). The solid circles plot the electron kinetic energy, $E_{\rm kin}(t)$. From this figure, we see the following characteristics of the HHG energy properties. (i) A few-cycle laser can produce a packet of sub-fs pulses. Its duration is equivalent to the duration of the laser pulse. (ii) Several harmonics of different energies can be generated at the same time, and are radiated by electrons with different return times, $\tau_{\rm st}$. (iii) The HHG cutoff energy $E_0(3.0U_{\rm p}) + I_{\rm p}$ for the laser with $\tau_{\rm L} = 7$ fs and $\Phi = 0°$ is less than $3.17U_{\rm p} + I_{\rm p}$, which is often used to estimate the highest energy of HHG (cutoff law). (iv) There is only one distribution pulse between $E_1(2.6U_{\rm p})$ and $E_0(3.0U_{\rm p})$ (pure single distribution pulse). (v) The pure single distribution pulse is peaked at $t_0 = 0.49$ fs, spanned 0.36 fs (duration between $t_1 = 0.31$ fs and $t_2 = 0.67$ fs). (vi) Two neighbouring distribution pulses are separated by approximately half of the laser optical cycle.

Figure 1(c) shows the stationary points of different values of t' and t. Point G is identical to that in (a). Figure 1(d) is an expanded area of Fig. 1(c). The highlighted curve (from $t = t_1$ to t_2) denotes the temporal localization of the pure single distribution pulse.

2.3. Time properties of a single XUV pulse

We are interested in the pure single distribution pulse (shown in Fig. 1(b), selected with $E_{\rm kin}/U_{\rm p} > 2.6$). Figures 2(a)–2(c) depict the time properties of this pulse. The solid line in Fig. 2(a) plots the electron birth (ionization) time, t', vs. recombination (radiation) time, t, and is almost a straight line. The solid line in Fig. 2(b) plots the return time, $\tau = t - t'$, vs. t, and is also straight. The line of solid circles in Fig. 2(c) depicts the electron energy gain, $E_{\rm kin}(t)$, vs. t. The solid line is a Gaussian fit of $E_{\rm kin}(t)/U_{\rm p}$, $H(t) = 1.36 + 1.64\exp[-8.27(t-0.49)^2]$. They meet very well. Here, the electron birth time, t', and the recombination time, t, as well as the return time, τ, are expressed as the averages of contributions from all atoms.

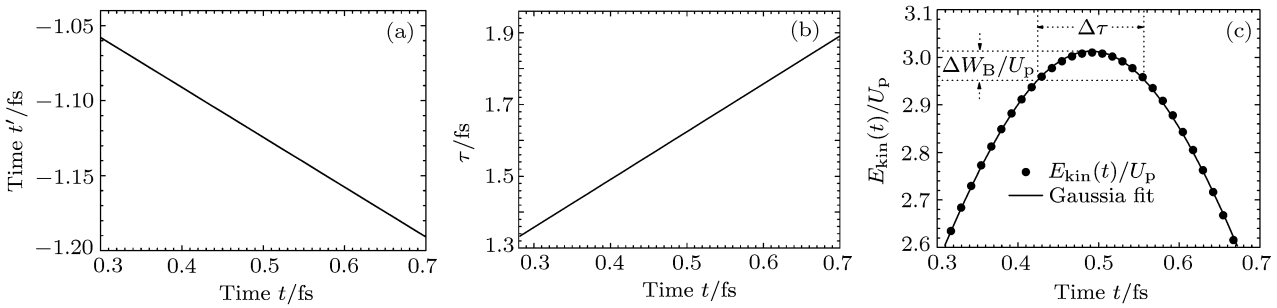


Fig. 2. Time properties of a pure single distribution pulse (selected with $E_{\rm kin}/U_{\rm p} > 2.6$). (a) Solid line: electron birth (ionization) time t' vs. recombination (radiation) time t. (b) Solid line: return time $\tau = t - t'$ vs. t. (c) Line of solid circles: electron energy gain $E_{\rm kin}(t)$ vs. t. Solid line: a Gaussian fit of $E_{\rm kin}(t)$.

For a small bandwidth, $\Delta W_{\rm BW}$ (eV), we can calculate the duration, $\Delta\tau$ (fs), of a selected pulse as follows:

$$\Delta\tau = 0.188\sqrt{\frac{\Delta W_{\rm BW}}{U_{\rm p}}}. \tag{3}$$

Equation (3) is derived from $H(t)$ close to the peak of the single distribution pulse (Fig. 2(c)). This equation can be used to estimate the duration of the selected XUV pulse at the cutoff energy. Equation (3) indicates that the bandwidth must be small and the laser intensity must be high in order to obtain a short as XUV pulse. As the laser duration increases to infinity, the pure single distribution pulse disappears, but a pulse train appears. Calculation shows that the HHG cutoff energy is $E_{\rm max} = 3.17U_{\rm p} + I_{\rm p}$, and that we can estimate the duration (fs) of each selected pulse with the bandwidth $\Delta W_{\rm BW}$ as $\Delta\tau = 0.179\sqrt{\Delta W_{\rm BW}/U_{\rm p}}$.

2.4. HHG energy properties by a $\tau_{\rm L} = 7$ fs 750-nm laser at $\Phi = 15°$ and $\Phi = 105°$

Figures 3(a) and 3(b) plot the HHG energy properties calculated for a 750-nm laser with $\tau_{\rm L} = 7$ fs, $\Phi = 15°$ and 105°, respectively. Figure 3(a) shows a single distribution pulse peaked at $t_0 = 0.38$ fs and spanned 0.42 fs. The pulse has a symmetric shape and a bandwidth of $E_0(3.0U_{\rm p}) - E_1(2.6U_{\rm p}) = 0.4U_{\rm p}$. Two side pulses of the same height between $E_0(3.0U_{\rm p})$ and $E_3(2.1U_{\rm p})$ are peaked at $t = -0.84$ fs and 1.59 fs, spanned 0.42 fs and 0.43 fs, respectively.

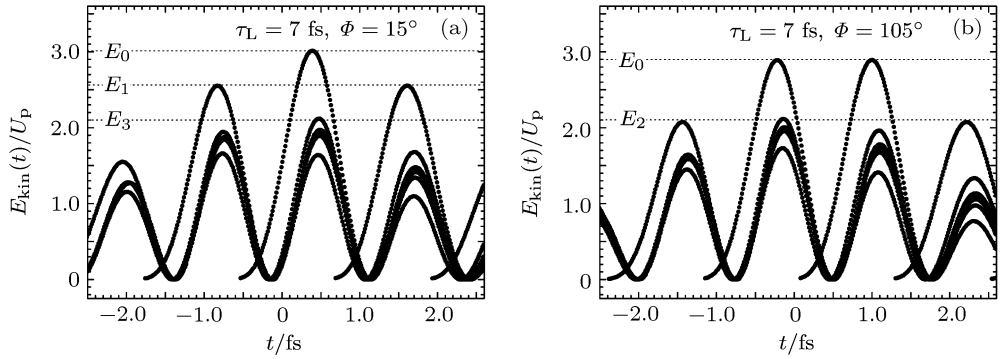


Fig. 3. (a) HHG energy properties calculated for a 750-nm laser with $\tau_{\rm L} = 7$ fs and $\Phi = 15°$. (b) HHG energy properties calculated for a 750-nm laser with $\tau_{\rm L} = 7$ fs and $\Phi = 105°$.

Two neighbouring distribution pulses are separated by 1.22 fs (about half of the laser optical cycle). Figure 3(b) shows a double-pulse structure between $E_0(2.9U_p)$ and $E_1(2.1U_p)$ (bandwidth of $0.8U_p$). Two pulses are peaked at -0.24 fs and 1.00 fs, spanned 0.54 fs and 0.55 fs, respectively. They are separated by 1.24 fs (half of the laser optical cycle), a time interval that reflects an intrinsic characteristic of HHG.

2.5. Laser-duration dependence of HHG energy properties

Figures 4(a) and 4(b) show the laser-duration dependences of the HHG energy properties, calculated for a 750-nm laser with $\Phi = 0°$ and different durations. Heavy solid and dash lines in Fig. 4(a) are values of E_0 and E_1 (see Fig. 1(b)) as functions of laser duration, respectively. Dash-dot line is the bandwidth $(E_0 - E_1)$. Dot line denotes the limitation position of $E_{max} = 3.17U_p$. Dash, heavy solid and thin solid lines in Fig. 4(b) are values of t_1, t_0 and t_2 (see Fig. 1(b)) as functions of laser duration, respectively. Dash-dot line is the duration of $(t_2 - t_1)$. Dot line denotes the limitation position of 0.50 fs. These results indicate that both the cutoff energy and the pulse localization go to their limitation positions as laser duration grows.

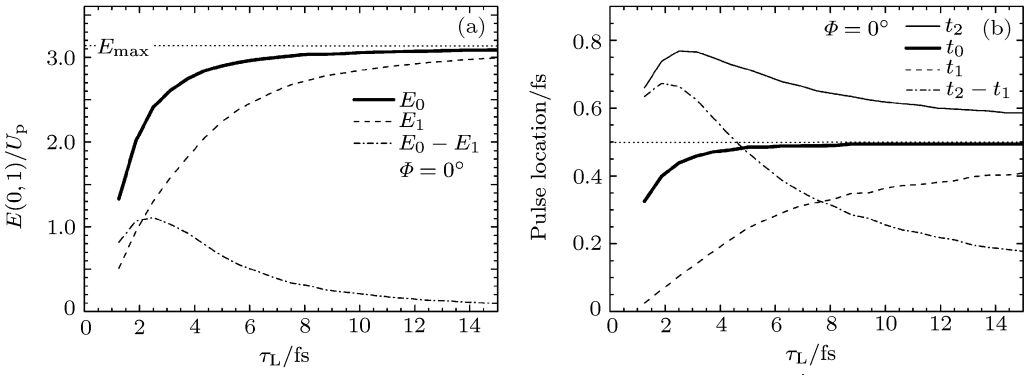


Fig. 4. Laser-duration dependences of the maximal kinetic energy E_0 (a) and the pulse localization (b), calculated for $\Phi = 0°$ 750-nm lasers. (a) Heavy solid and dash lines: values of E_0/U_p and E_1/U_p (see Fig. 1(b)), respectively. Dash-dot line: the bandwidth $(E_0 - E_1)/U_p$. E_{max} denotes the limitation value of $3.17U_p$. (b) Dash, heavy solid and thin solid lines: values of t_1, t_0 and t_2 (see Fig. 1(b)), respectively. Dash-dot line: the duration of $t_2 - t_1$.

Figures 4(a) and 4(b) show that the cutoff energy of HHG spectrum generated by a few-cycle laser is obviously less than that $(E_{max} = 3.17U_p + I_p)$ by a laser for infinite duration. At $\tau_L \approx 2$ fs, the bandwidth $(E_0 - E_1)$ and the pulse duration $(t_2 - t_1)$ reach their maximal values separately. As the laser duration grows, the bandwidth of the single distribution pulse decreases quickly to zero but its duration decreases slowly to 0.17 fs or less.

2.6. CEP dependence of HHG energy properties

Calculations demonstrate that the HHG energy properties depend not only on the laser duration, but also on the laser intensity and CEP. Herein, we present some results of the CEP dependence.

Figures 5(a) and 5(b) depict the CEP dependence of the cutoff energy and the time localization of the pure single distribution pulse, calculated for a 750-nm $\tau_L = 7$ fs laser. The heavy solid and dash lines in Fig. 5(a) are values of E_0 and E_1 (see Fig. 1(b)), respectively. The dot line is the bandwidth of $E_0 - E_1$. The dash, heavy solid and thin solid lines in Fig. 5(b) plot the values of t_1, t_0, and t_2 (see Fig. 1(b)) as CEP varies, respectively. The dot line is the duration of $t_2 - t_1$. Both the cutoff energy and the duration of the pure single distribution pulse depict periodic structures (repeated for 180° in CEP domain). For example, the bandwidth, the cutoff energy, and the duration of the pulse achieve their maximal values at $\Phi = -165°$, 15°, 195°, etc. They have minimal values at $\Phi = -255°$, $-75°$, 105°, 285°, etc. At these CEPs, e.g. $\Phi = -75°$, the lines of t_1, t_0, and t_2 are folded because the highest pulse and the second highest pulse exchange their temporal positions.

As CEP varies, the cutoff energy changes slightly, but both the bandwidth and the duration of the pure single distribution pulse change significantly. From the plots in Fig. 5(b), we see that the temporal position, t_0, of the pure single distribution pulse linearly follows the change of CEP in each 180° range. This is an interesting feature that may be used to temporally control the selected attosecond pulse by changing CEP.

Figures 5(c) and 5(d) show the CEP dependence of HHG energy properties, calculated for a $\tau_{\rm L} = 5$ fs 750-nm laser. Although the values of E_0, E_1, t_1 and t_2 are different from those in Figs. 5(a) and 5(b) at a specified CEP, the temporal positions of maximal/minimal E_0 and E_1 are almost the same as those in Figs. 5(a) and 5(b). The range of t_0 in each 180° periodic structure is half of the laser optical cycle.

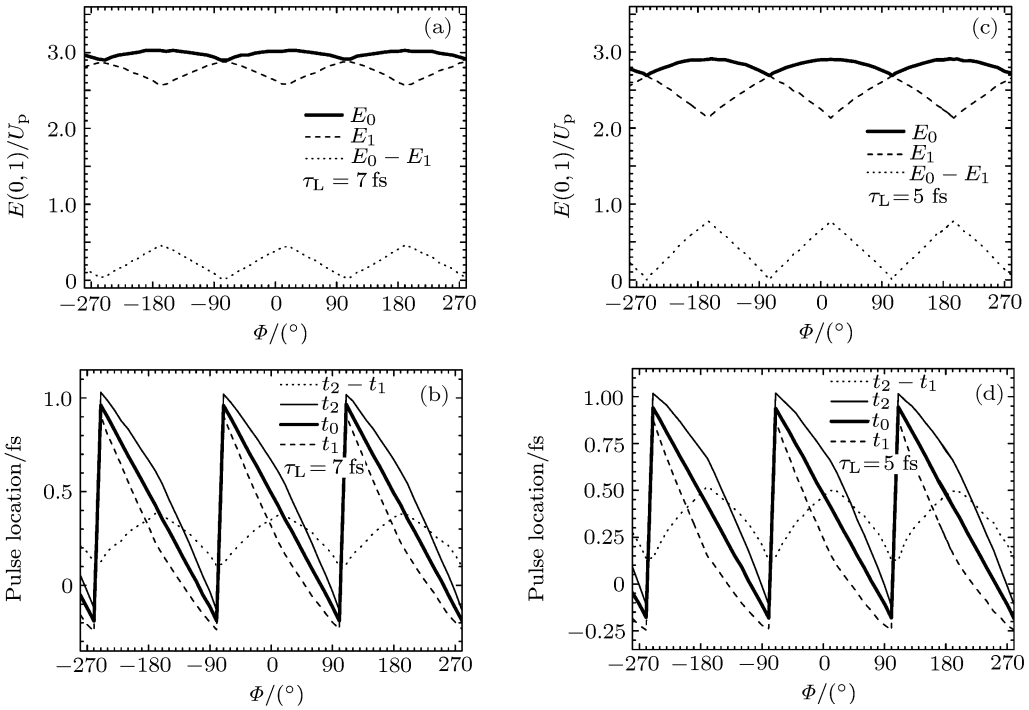


Fig. 5. CEP dependence of the cutoff energy and the temporal localization of pure single distribution pulse of the HHG radiation properties generated by a $\tau_{\rm L} = 7$ fs 750-nm laser. (a) Heavy solid and dash lines: values of E_0 and E_1 (see Fig. 1(b)), respectively. Dot line: the bandwidth of $E_0 - E_1$. (b) Dash, heavy solid, and thin solid lines: values of t_1, t_0, and t_2 (see Fig. 1(b)), respectively. Dot line: the duration of $t_2 - t_1$. (c) and (d) Similar to (a) and (b), the CEP dependence of the maximal kinetic energy E_0 (c) and the pulse localization t_1, t_0, and t_2 (d), calculated for a $\tau_{\rm L} = 5$ fs 750-nm laser.

3. Detection of a narrowband as XUV pulse

The above calculations have quantitatively demonstrated that an as XUV pulse can be isolated with a bandpass optical filter, but many factors affect the detection of this pulse, such as laser beam size, pulse spatiotemporal reshaping in the gas,[13] the propagation of the generated XUV pulse, etc. Here, we first give an estimation of the influence of the beam size on the result, and then discuss those resulting from the instability and fluctuation of the laser intensity and CEP.

Figure 6(a) illustrates the detection of an isolated single XUV pulse. The space within dash lines represents the region of the laser beam where the intensity is approximately uniform. There are three points denoted by A, B, and C. Their space coordinates are $(0, 0, z_1)$, $(0, y_1, z_1)$, and $(0, 0, z_2)$, respectively. The detector is placed at point $D(0, 0, z_3)$. Points A, C, and D are in the Z axis, while point B has a small distance, y_1 ($\ll z_3 - z_1$, in the Y axis), from point A. ω_1 and ω_2 (solid lines) represent pure distribution pulses shown in Fig. 2(c) generated by atoms at point A and point C, respectively. The pure distribution pulse generated at point B is the same as ω_1.

The ω_3 (solid line) and ω_4 (dash-dot line) are detected pulses generated at points A and B, respectively. On the assumption that the laser pulse reaches point A at time t, and the ionization for HHG takes place, the atom will radiate a harmonic photon after a return time τ. This photon will reach point D at time $t+(z_3-z_1)/c+\tau$. Similarly, the laser pulse reaches point C at time $t+(z_2-z_1)/c$, and will radiate a photon after time τ. This photon will reach point D at time $t+(z_3-z_1)/c+\tau$, the same as that of the photon from point A. Different from the photons from points A and C, the photon from point B will reach the point D at time $t+(z_3-z_1+\delta)/c+\tau$ (denoted by point E), where $\delta=\sqrt{(y_1)^2+(z_3-z_1)^2}-(z_3-z_1)$. Obviously, D and E are the same point in space but they have different times. The detected pulse ω_4 is delayed from ω_3 by δ/c. Therefore the final detected pulse will be the sum of $\omega_3+\omega_4+\cdots$. Hence, this describes the influence of laser beam size on the measurement. For example, with a beam diameter of 1 mm ($y_1 \leq 0.5$ mm) and $z_3-z_1=3000$ mm, the small value $\delta \leq 0.0417$ μm and the time delay $\delta_t=\delta/c \leq 139.1$ as, which is a large value for an as pulse. However, with $y_1 \leq 0.05$ mm and $z_3-z_1=3000$ mm, we have $\delta_t=\delta/c \leq 1.39$ as, a small value that can be neglected. This indicates that the strong spatiotemporal reshaping of the laser pulse[13] slightly affects the result measured with these parameters. Experimentally, when $y_1 \ll (z_3-z_1)$ and the small time $\delta/c \approx (y_1)^2/2c(z_3-z_1)$ less than, e.g. 5 as, the influence of laser beam size and pulse reshaping on the measurement can be approximately removed from consideration.

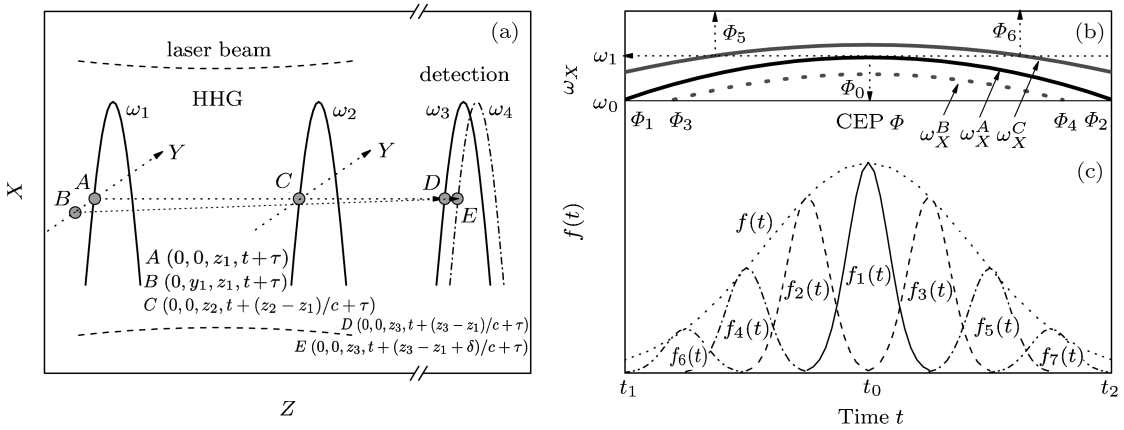


Fig. 6. (a) Detection of isolated single XUV pulses. The first three numbers in the brackets A through E are the space coordinates and the fourth numbers are the times of atomic ionizations (A, B, C) or photon detections (D, E). (b) Illustrations of the fluctuations and walks of laser intensity and CEP. (c) (Below Fig. 6(b)) The effects of laser intensity instability and CEP instability on the result of the measured single XUV pulse.

Figure 6(b) illustrates the influence of fluctuations and walks of laser intensity and CEP on the measurement. ω_X^A (heavy solid line), ω_X^B (grey heavy dot line), and ω_X^C (grey heavy solid line) are the CEP dependence of the HHG energy properties at different laser intensities (corresponding to middle, low, and high intensity values of the fluctuations). As we use a narrow bandpass filter to measure the isolated pulses, only those photons that have energies within ω_0 and ω_1 will be detected. Φ_0 denotes the central value of the CEP fluctuations (from Φ_1 to Φ_2). Limited by the filter, only those photons that have CEPs ranging from Φ_3 to Φ_4 (ω_X^B) can be detected at low laser intensity, and photons with CEPs from Φ_1 to Φ_5 and from Φ_6 to Φ_2 (ω_X^C) can be detected at high laser intensity. Similarly, all photons with CEPs from Φ_1 to Φ_2 (ω_X^A) can be detected at a middle laser intensity.

Figure 6(c) (below Fig. 6(b)) depicts the influence of laser intensity instability and CEP instability on the result of the measured single XUV pulse. Since we use a narrow bandpass filter, each laser pulse produces a short duration XUV pulse according to Eq. (3), e.g. $f_i(t)$ ($i=1, 2, \ldots, 7$) shown in the figure, where each corresponds to an instantaneous laser intensity and a CEP. The final result of the measured pulse will be the sum of these pulses, $f(t)=\sum f_i(t)$, $i=1, 2, \ldots$ (shown by thin dotted line), which reflect the distributions

(of fluctuations and walks) of laser intensity and CEP. These features are useful for laser beam control and optimization of the selected XUV pulse.

4. Summary

The calculated HHG time-energy properties provide new references for producing, selecting, improving, and manipulating as pulses. The CEP dependence of the HHG energy properties depict interesting 180° periodic structures. The calculations and analyses demonstrate that a narrowband as XUV pulse can be selected by using a narrow bandpass optical filter from HHG spectrum near the cut-off energy. The theoretical prediction of the pulse duration is proportional to the bandwidth. The measured pulse may include instantaneous short duration pulses, whose time properties depend on laser intensity, CEP fluctuation, and walk.

Acknowledgment

The authors acknowledge Ge Xiang-Jie for assistance.

References

[1] Drescher M, Hentschel M, Kienberger R, Tempea G, Spielmann C, Reider G A, Corkum P B and Krausz F 2001 *Science* **291** 1923

[2] Hentschel M, Kienberger R, Spielmann C, Reider G A, Milosevic N, Brabec T, Corkum P B, Heinzmann U, Drescher M and Krausz F 2001 *Nature* (London) **414** 509

[3] Drescher M, Hentschel M, Kienberger R, Uiberacker M, Yakovlev V, Scrinzi A, Westerwalbesloh T, Kleineberg U, Heinzmann U and Krausz F 2002 *Nature* (London) **419** 803

[4] Kienberger R, Goulielmakies E, Uiberacker M, Baltuska A, Yakovlev V, Bammer F, Scrinzi A, Westerwalbesloh T, Kleineberg U, Heinzmann U, Drescher M and Krausz F 2004 *Nature* (London) **427** 817

[5] Goulielmakis E, Uiberacker M, Kienberger R, Baltuska A, Yakovlev V, Scrinzi A, Westerwalbesloh T, Kleineberg U, Heinzmann U, Drescher M and Krausz F 2004 *Science* **305** 1267

[6] Sansone G, Benedetti E, Calegari F, Vozzi C, Avaldi L, Flammini R, Poletto L, Villoresi P, Altucci C, Velotta R, Stagira S, Silvestri S D and Nisoli M 2006 *Science* **314** 443

[7] Spielmann C and Burnett N H 1997 *Science* **278** 661

[8] Schnürer M, Spielmann C, Wobrauschek P, Streli C, Burnett N H, Kan C, Ferencz K, Koppitsch R, Cheng Z, Brabec T and Krausz F 1998 *Phys. Rev. Lett.* **80** 3236

[9] Kienberger R, Goulielmakis E, Uiberacker M, Baltuska A, Drescher M and Krausz F 2005 *J. Mod. Opt.* **52** 261

[10] Scrinzi A, Ivanov M U, Kienberger R and Villeneuve D M 2006 *J. Phys.* B: *At. Mol. Opt. Phys.* **39** R1

[11] Cavalieri A , Müller N, Uphues T, Yakovlev V S, Baltuka A, Horvath B, Schmidt B, Blümel L, Holzwarth R, Hendel S, Drescher M, Kleineberg U, Echenique P M, Kienberger R, Krausz F and Heinzmann U 2007 *Nature* **449** 1029

[12] Mairesse Y, Bohan A D, Frasinski L J, Merdji H, Dinu L C, Monchicourt P, Breger P, Kovačev M, Auguste T, Carré B, Muller H G, Agostini P and Salières P 2004 *Phys. Rev. Lett.* **93** 163901

[13] Gaarde M B and Schafer K J 2006 *Opt. Lett.* **31** 3188

[14] Schiessl K, Ishikawa K L, Persson E and Burgdörfer J 2007 *Phys. Rev. Lett.* **99** 253903

[15] Goulielmakis E, Schultze M, Hofstetter M, Yakovlev V S, Gagnon J, Uiberacker M, Aquila A L, Gullikson E M, Attwood D T, Kienberger R, Krausz F and Kleineberg U 2008 *Science* **320** 1614

[16] Ge Y C 2006 *Phys. Rev.* A **74** 015803

[17] Ge Y C 2008 *Phys. Rev.* A **77** 033851

[18] Ge Y C 2005 *Acta Phys. Sin.* **54** 2653 (in Chinese)

[19] Ge Y C 2005 *Acta Phys. Sin.* **54** 2669 (in Chinese)

[20] Ge Y C 2006 *Acta Phys. Sin.* **55** 3386 (in Chinese)

[21] Ge Y C 2005 *Chin. Phys. Lett.* **22** 349

[22] Ge Y C 2005 *Chin. Phys. Lett.* **22** 1916

[23] Ge Y C 2006 *Chin. Phys. Lett.* **23** 143

[24] Ge Y C 2006 *Chin. Phys.* **15** 2909

[25] Ge Y C 2008 *Chin. Phys.* B **17** 2072

[26] Ge Y C 2008 *Chin. Phys.* B **17** 4492

[27] Ge Y C 2009 *Chin. Phys.* B **18** 1473

[28] Potvliege R M, Kylstra N J and Joachain C J 2000 *J. Phys.* B: *At. Mol. Opt. Phys.* **33** L743

[29] Corkum P B and Krausz F 2007 *Nature Phys.* **3** 381

[30] Nisoli N and Sansoni G 2009 *Prog. Quantum Electron.* **33** 17

[31] Lewenstein M, Balcou P, Ivanov M Y, LHuillier A and Corkum P B 1994 *Phys. Rev.* A **49** 2117